



# A Shift in Central Metabolism Accompanies Virulence Activation in *Pseudomonas aeruginosa*

Kumar Perinbam,<sup>a</sup> Jenu V. Chacko,<sup>b</sup> Anerudh Kannan,<sup>a</sup> Michelle A. Digman,<sup>b</sup> Albert Siryaporn<sup>a,c</sup>

<sup>a</sup>Department of Physics and Astronomy, University of California, Irvine, Irvine, California, USA

<sup>b</sup>Department of Biomedical Engineering, University of California, Irvine, Irvine, California, USA

<sup>c</sup>Department of Molecular Biology and Biochemistry, University of California, Irvine, Irvine, California, USA

Kumar Perinbam and Jenu V. Chacko contributed equally to this work. Authors are in order of increasing seniority.

**ABSTRACT** The availability of energy has significant impact on cell physiology. However, the role of cellular metabolism in bacterial pathogenesis is not understood. We investigated the dynamics of central metabolism during virulence induction by surface sensing and quorum sensing in early-stage biofilms of the multidrug-resistant bacterium *Pseudomonas aeruginosa*. We established a metabolic profile for *P. aeruginosa* using fluorescence lifetime imaging microscopy (FLIM), which reports the activity of NADH in live cells. We identified a critical growth transition period during which virulence is activated. We performed FLIM measurements and direct measurements of NADH and NAD<sup>+</sup> concentrations during this period. Here, planktonic (low-virulence) and surface-attached (virulence-activated) populations diverged into distinct metabolic states, with the surface-attached population exhibiting FLIM lifetimes that were associated with lower levels of enzyme-bound NADH and decreasing total NAD(H) production. We inhibited virulence by perturbing central metabolism using citrate and pyruvate, which further decreased the enzyme-bound NADH fraction and total NAD(H) production and suggested the involvement of the glyoxylate pathway in virulence activation in surface-attached populations. In addition, we induced virulence at an earlier time using the electron transport chain oxidase inhibitor antimycin A. Our results demonstrate the use of FLIM to noninvasively measure NADH dynamics in biofilms and suggest a model in which a metabolic rearrangement accompanies the virulence activation period.

**IMPORTANCE** The rise of antibiotic resistance requires the development of new strategies to combat bacterial infection and pathogenesis. A major direction has been the development of drugs that broadly target virulence. However, few targets have been identified due to the species-specific nature of many virulence regulators. The lack of a virulence regulator that is conserved across species has presented a further challenge to the development of therapeutics. Here, we identify that NADH activity has an important role in the induction of virulence in the pathogen *P. aeruginosa*. This finding, coupled with the ubiquity of NADH in bacterial pathogens, opens up the possibility of targeting enzymes that process NADH as a potential broad antivirulence approach.

**KEYWORDS** FLIM, PilY1, antivirulence, central metabolism, fluorescence lifetime imaging microscopy, quorum sensing, surface sensing, virulence regulation

*Pseudomonas aeruginosa* is an opportunistic pathogen that is responsible for a range of illnesses, including lung infections in cystic fibrosis patients and hospital-acquired infections, sepsis, and disease in immunocompromised patients (1). The bacterium infects a broad range of hosts, including humans, animals, plants, insects,

**Citation** Perinbam K, Chacko JV, Kannan A, Digman MA, Siryaporn A. 2020. A shift in central metabolism accompanies virulence activation in *Pseudomonas aeruginosa*. mBio 11:e02730-18. <https://doi.org/10.1128/mBio.02730-18>.

**Editor** Joanne Engel, University of California, San Francisco

**Copyright** © 2020 Perinbam et al. This is an open-access article distributed under the terms of the [Creative Commons Attribution 4.0 International license](https://creativecommons.org/licenses/by/4.0/).

Address correspondence to Albert Siryaporn, [asirya@uci.edu](mailto:asirya@uci.edu).

**Received** 18 December 2019

**Accepted** 28 January 2020

**Published** 10 March 2020

amoebae, and other bacteria using a multitude of virulence factors, including the type III secretion system, cyanide, pyocyanin, and proteases (2–5). Recent work has reported that the expression of virulence factors in *P. aeruginosa* is regulated by nutrient availability and central metabolic networks (6–8). In addition, tricarboxylic acid cycle (TCA) intermediates alter the activity of some virulence factor regulators in Gram-positive and intracellular pathogens (9, 10). These studies provide a static snapshot of the involvement of metabolism in virulence regulation. The dynamics of central metabolic activity during the activation of virulence in *P. aeruginosa* are not known, and many questions remain about the regulatory link between central metabolism and virulence activation. What are the energetic requirements for the expression of virulence factors? Can central metabolism be tuned to inhibit virulence? We investigated these questions by measuring central metabolic activity during the transition from a low-virulence state to an activated virulence state in *P. aeruginosa*.

Virulence factor production is induced in *P. aeruginosa* and other bacteria through the activation of surface sensing (11–15). The host-killing mechanism of surface-activated virulence in *P. aeruginosa* has not been attributed to a single virulence factor, including a type III secretion product, pyocyanin, or elastase, but has been attributed to the combinatorial nature of virulence factor production (2, 12). A recent preprint reports that alkyl quinolones are a critical cytotoxic factor (16). Virulence induction by surface attachment is dependent on the protein PilY1, which is found on the outer surface of the cell membrane, contains homology to a mechanically active von Willebrand factor domain, mediates a c-di-GMP response to shear stress, and is required for the initiation of biofilm formation (17–21). Surface-induced virulence also requires coactivation of quorum sensing, which is triggered when cells reach a threshold density (22, 23). Surface sensing and quorum sensing form a coincidence gate in which the activation of both pathways is required to induce virulence (12).

Surface attachment regulates the levels of the metabolites cyclic AMP and cyclic di-GMP (13, 20, 21, 24) and upregulates transcription of NADH-associated enzymes (12). Quorum sensing, which controls the expression of many virulence factors, produces a major shift in the production of a large fraction of metabolites (25). It is possible that surface sensing and quorum sensing induce virulence through changes in central metabolism. However, addressing this hypothesis has been challenging because surface sensing and quorum sensing are dynamic processes and monitoring their effects requires simultaneous measurements of both virulence and central metabolism.

The phasor approach to fluorescence lifetime imaging microscopy (FLIM) measures the dynamics of central metabolism in live cells. This method reports the relative abundance of the free and bound forms of NADH by exploiting its autofluorescent properties (26, 27). This method has been used extensively to track changes in NADH forms in live eukaryotic cells during critical cell processes, including duplication, proliferation, and differentiation (28–32). NADH is excited using two-photon excitation and decays to the ground state with distinct decay rates, or lifetimes, in the visible spectrum. The major advantage of this approach is the ability to track spatial and temporal changes in metabolic activity at subcellular resolution without the need to label molecules, introduce fluorescent reporters, or to stain, perturb, or harvest cells. Advances in optics, imaging, and analysis have enabled fluorescence lifetime measurements in a number of bacteria, including *Lactobacillus acidophilus*, *Escherichia coli*, and *P. aeruginosa* (33–37). However, independent measurements of NADH were not performed in these studies, which limited the interpretation of the FLIM measurements. In addition, the FLIM measurements were not performed during virulence activation.

Here, we establish a metabolic trajectory in *P. aeruginosa* using FLIM and through independent *in vitro* measurements of NADH and NAD<sup>+</sup> concentrations. We measure metabolic states in *P. aeruginosa* during a critical growth transition in which virulence is activated in surface-attached cells. We show that compared to low-virulence (planktonic) cells, virulence-activated (surface-attached) cells exhibit FLIM lifetimes that are associated with decreased levels of enzyme-bound NADH and decreased NAD(H) production. Perturbation of central metabolism using citrate or pyruvate, which further

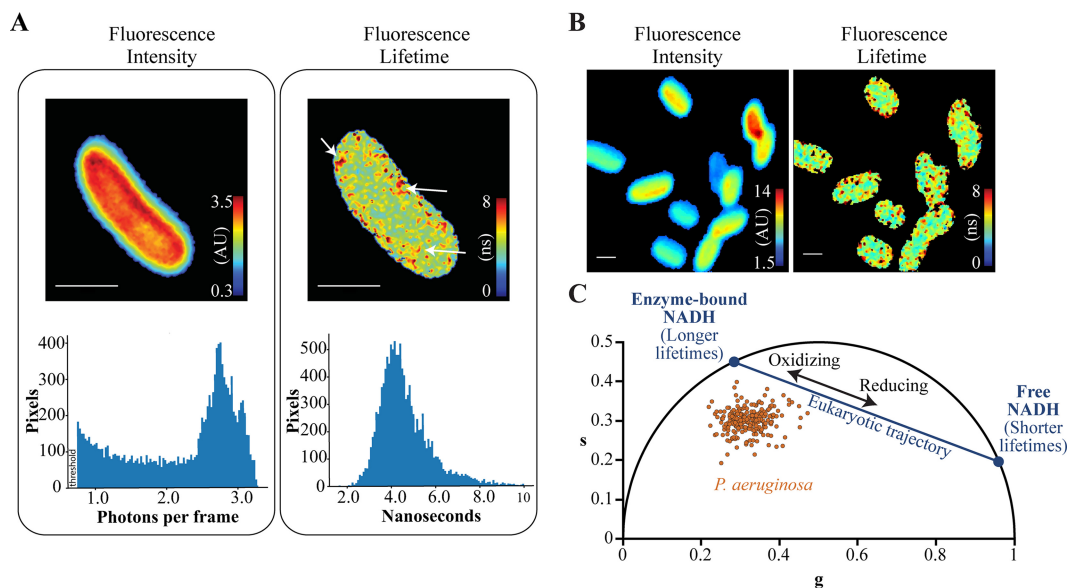


**FIG 1** Metabolic profiling of live planktonic *P. aeruginosa* cells using fluorescence lifetime imaging microscopy. (A) Fluorescence intensities (in arbitrary units [AU]) and fluorescence lifetimes (in nanoseconds) of an unlabeled *P. aeruginosa* cell imaged using the NADH emission spectrum. The corresponding fluorescence intensity and lifetime histograms are displayed below the images. Arrows indicate clusters with relatively long fluorescence lifetimes. Bars, 1  $\mu\text{m}$ . (B) Fluorescence intensities and lifetimes of multiple *P. aeruginosa* cells. Bars, 1  $\mu\text{m}$ . (C) Phasor plot in which the cosine and sine components of the fluorescence lifetime are transformed into  $g$  and  $s$  coordinates, respectively. Each dot represents the fluorescence lifetime averaged over an individual *P. aeruginosa* cell. The metabolic trajectory of eukaryotic cells is plotted for reference using lifetime values of 0.4 ns and 3.4 ns for free and protein-bound NADH, respectively. Planktonic *P. aeruginosa* from three independent experiments were cultured to early exponential phase in modified minimal medium containing 0.2% citrate as the carbon source.

decreases enzyme-bound NADH and total NAD(H) production, inhibits virulence, while treatment using an electron transport chain oxidase inhibitor induces virulence at an earlier time.

## RESULTS

**Fluorescence lifetimes shift with changes in NAD(H) production in *P. aeruginosa*.** We measured the fluorescence intensities and lifetimes of unlabeled wild-type *P. aeruginosa* using two-photon microscopy with excitation at 740 nm and emission centered at 460 nm with an 80-nm bandwidth (NADH emission spectrum). Studies of eukaryotic cells have established that fluorescence intensity is proportional to the concentration of intracellular NADH or NADPH and that fluorescence lifetime is determined by the relative fraction of NADH or NADPH that is free or bound to proteins (28–31, 38–41). The fluorescence lifetimes of NADH and NADPH are indistinguishable using the techniques in this study, and thus, we do not differentiate between these species and refer to NADH only. We cultured *P. aeruginosa* in minimal medium and measured fluorescence at mid-exponential phase. Fluorescence intensities were uniformly distributed in the cytoplasmic region of the cell and dropped off sharply at the periphery (Fig. 1A and B). In contrast, fluorescence lifetimes were relatively heterogeneous within the cytoplasm, and longer fluorescence lifetimes were localized to multiple clusters within the cell (Fig. 1A and B).

We analyzed fluorescence lifetimes using the phasor approach, which determines the relative fraction of free and enzyme-bound forms of NADH and is insensitive to the total intracellular concentration of NADH (26, 27). In this approach, fluorescence decay curves are transformed by cosine and sine functions and plotted along  $g$  and  $s$  axes, respectively. Fluorescence lifetimes that arise from a single species map to the “universal circle” of the phasor (26, 27) (black semicircle in Fig. 1C). Free (unbound) NADH has a relatively short lifetime (0.4 ns) and maps to a coordinate on the lower right region of the universal circle (Fig. 1C). NADH molecules that are bound to eukaryotic

enzymes have longer lifetimes (3.2 to 9 ns) and map to coordinates on the upper left region of the universal circle (28, 29, 39, 40) (Fig. 1C). The positions of free and enzyme-bound NADH on the universal circle serve as reference points. Lifetime decay curves that are generated by a mixture of free and enzyme-bound NADH species, which is typically observed in fluorescence lifetime measurements that are averaged over entire eukaryotic cells, map along a linear trajectory that connects the two reference points on the universal circle (28, 29, 40) (Fig. 1C).

Previous studies of eukaryotic cells demonstrate that growth under oxidizing conditions, which decreases the relative free NADH pool and the ratio of free to enzyme-bound NADH, results in increased fluorescence lifetimes and phasor positions that are further away from the free NADH reference point (28–30) (Fig. 1C). Conversely, growth in a reducing environment or blocking oxidative phosphorylation through metabolic inhibitors, both of which increase the relative free NADH pool, results in decreased lifetimes and phasor positions that are closer to the free NADH reference (28–30) (Fig. 1C). These studies establish that the position of lifetimes along the linear trajectory is an indicator of the relative abundance of free and enzyme-bound NADH within the cell.

In our experiments, *P. aeruginosa* cells mapped outside of the eukaryotic NADH trajectory (Fig. 1C). The central metabolic enzymes that bind NADH in *P. aeruginosa* and eukaryotes are distinct (42, 43), and thus, there is no expectation that fluorescence lifetimes for eukaryotes and bacteria should appear along the same trajectory. To establish a metabolic trajectory for *P. aeruginosa*, we cultured cells in minimal media supplemented with single carbon sources that are associated with different levels of NADH production. Citrate is metabolized through the tricarboxylic acid cycle (TCA) cycle, which reduces  $\text{NAD}^+$  to NADH (Fig. 2A). Glycerol and glucose are metabolized through the Entner-Doudoroff pathway, which produces NADH molecules and pyruvate, the latter of which can enter the TCA cycle (42–44). We expected that the metabolism of citrate, glycerol, glucose, or pyruvate would produce different levels of NADH (Fig. 2A).

We quantified the concentrations of intracellular NADH and  $\text{NAD}^+$  in surface-attached cells that were cultured in each of the carbon sources (Fig. 2B to D) using an enzyme-cycling-based colorimetric assay (45, 46). This assay serves as an independent approach to measuring changes in NADH in addition to the FLIM technique. We observed that the assay was sensitive to the concentration of *P. aeruginosa* and therefore normalized samples by total protein concentration. We included measurements of a  $\Delta\text{phz1/2}$  strain, which does not produce pyocyanin, to identify the protein concentration required to measure changes in NADH and  $\text{NAD}^+$ . The NADH/ $\text{NAD}^+$  ratio of this strain increases significantly during the transition from early exponential to late exponential phase (46). The observed increase in ratio between these growth phases (Fig. 2B) established that the *P. aeruginosa* concentrations in our samples were within the dynamic range of the assay.

Consistent with expectations, we observed that each carbon source yielded a different NADH/ $\text{NAD}^+$  ratio (Fig. 2B). In particular, pyruvate produced the smallest ratio, whereas citrate, glycerol, and glucose yielded increasing ratios. The total concentrations of NADH and  $\text{NAD}^+$  were highest for pyruvate, intermediate for citrate and glycerol, and smallest for glucose (Fig. 2C). The changes in the NADH/ $\text{NAD}^+$  ratios and total concentrations of NAD(H) were primarily due to changes in  $\text{NAD}^+$  production, as the NADH concentrations were relatively constant (Fig. 2D).

We hypothesized that the changes in NADH/ $\text{NAD}^+$  ratios and NAD(H) concentrations are accompanied by changes in the relative fractions of enzyme-bound and free NADH, which would be observed as changes in fluorescence lifetime. We measured fluorescence lifetimes (at single-cell resolution) of surface-attached *P. aeruginosa* that were cultured under the same conditions as the NAD(H) measurements. We observed significant changes in fluorescence lifetimes primarily along the  $g$  axis (Fig. 2E). Growth using pyruvate yielded the smallest  $g$  value, whereas growth using citrate, glycerol, and glucose yielded increasing  $g$  values (Fig. 2E). Interestingly,  $g$  values anticorrelated

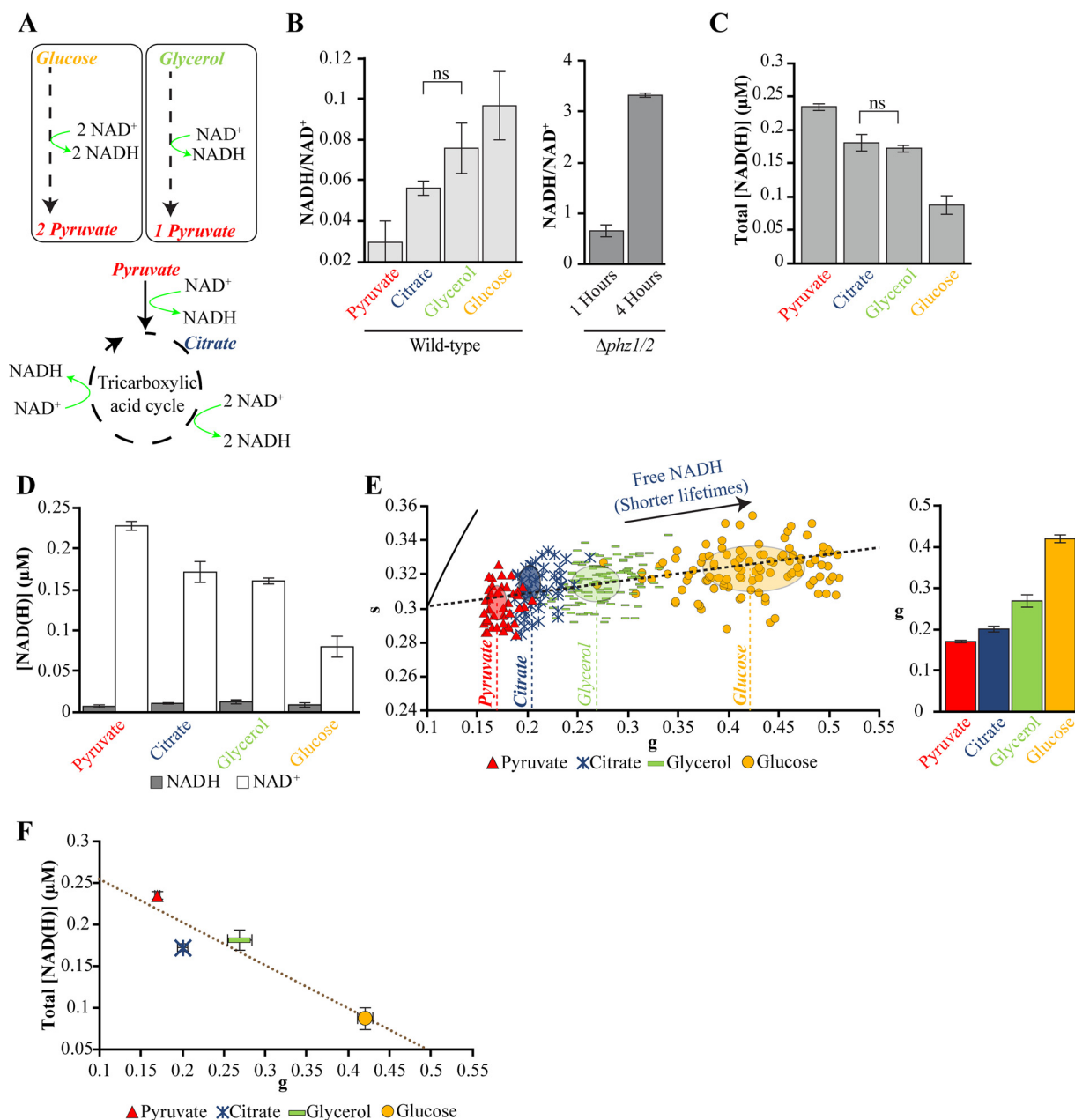


**FIG 2** Carbon sources alter NAD(H) concentrations and fluorescence lifetimes in surface-attached *P. aeruginosa*. (A) Schematic indicating the production of NADH by central metabolism pathways in *P. aeruginosa*. (B to D) Measurements of NADH/NAD<sup>+</sup> ratios (B), total NADH and NAD<sup>+</sup> production (C), and the concentration of NADH or NAD<sup>+</sup> measured using an enzyme-cycling assay using surface-attached *P. aeruginosa* cultured using single carbon sources at 0.2% (D). ns, not significant. Bars indicate the average values and error bars indicate the standard deviations from three independent experiments. (E) Fluorescence lifetime phasor plot (left) and corresponding *g* values (right) of *P. aeruginosa* cultured using identical conditions as the enzyme-cycling assay. Points on the map represent the average fluorescence lifetime of approximately five cells. The centers and axis lengths of the ellipses correspond to the mean and standard deviation, respectively, of all cells pooled from three independent experiments. The dashed line indicates a metabolic trajectory that connects the average phasor positions for different carbon sources. The arrow indicates the direction toward the position of the free NADH reference, which does not appear on this plot. The bars and error bars in the bar graph indicate the means and standard deviations of the means from three independent experiments, respectively. (F) Total NAD(H) concentrations and fluorescence lifetime *g* values for growth on single carbon sources. The points and error bars indicate the means and standard deviations of the means from three independent experiments, respectively. The best-fit line is indicated with  $R = -0.94$ . All measurements were made on surface-attached *P. aeruginosa* cells that were cultured in modified minimal medium and harvested at mid-exponential phase, with the exception of the  $\Delta phz1/2$  strain, which was cultured in modified MOPS medium and harvested at different phases. Full statistical details are given in Table S1 in the supplemental material.

(negatively correlated) with total NAD(H) concentrations (Fig. 2F) ( $R = -0.94$ ). To our knowledge, this relationship has not been identified previously for *P. aeruginosa*.

We repeated NAD(H) and fluorescence lifetime measurements using planktonic cells that were isolated from the same cultures as the surface-attached cells. The trends in NADH/NAD<sup>+</sup> ratios and total NAD(H) concentrations for these cells (see Fig. S1A to C in the supplemental material) were identical to those of surface-attached cells (Fig. 2B to D) with the exception that in planktonic cells, citrate produced a slightly greater NADH/NAD<sup>+</sup> ratio and slightly lower NAD(H) concentration than glycerol (Fig. S1A and B). However, the differences in NADH/NAD<sup>+</sup> ratios and total NAD(H) concentrations using citrate or glycerol as a carbon source in surface-attached cells were not significant (Fig. 2B and C). The trend in fluorescence lifetime  $g$  values in planktonic cells (Fig. S1D) was identical to that of surface-attached cells (Fig. 2E). Fluorescence lifetime  $g$  values and total NAD(H) concentrations in planktonic cells were also anticorrelated (Fig. S1E,  $R = -0.86$ ). These results indicate that the impacts of carbon sources on FLIM and NAD(H) production were qualitatively comparable for both planktonic and surface-attached *P. aeruginosa*. We note that the changes in NAD(H) concentrations in planktonic cells arose from changes in both NADH and NAD<sup>+</sup> (Fig. S1C), in contrast to surface-attached cells, where changes in only NAD<sup>+</sup> were observed (Fig. 2D).

The relative shifts in fluorescence lifetime are not due to pyoverdine or pyocyanin, which are fluorescent molecules produced in high abundance by *P. aeruginosa* (46, 47), because the lifetime shifts were observed in strains that are defective in the production of pyoverdine or pyocyanin (see Fig. S2A and B in the supplemental material). Purified forms of pyoverdine and pyocyanin also mapped to positions outside the *P. aeruginosa* lifetime range (Fig. S2C). Furthermore, a shift toward higher  $g$  value (greater fraction of free NADH) was observed when *P. aeruginosa* was treated with the oxidase inhibitor antimycin A, which inhibits electron transport chain activity (48, 49) (Fig. S2D). Together, these results establish a fluorescence lifetime metabolic activity trajectory for *P. aeruginosa* (Fig. 2E and Fig. S1D). In particular, the *P. aeruginosa* trajectory is positioned below the eukaryotic metabolic trajectory (Fig. S2C) on the phasor diagram, and the shifts are mostly along the  $g$  axis. These data indicate that the selection of carbon source affects total NAD(H) production and the relative fractions of free and enzyme-bound NADH. The observation that changes in NAD(H) production are anticorrelated with changes in fluorescence lifetime (Fig. 2F and Fig. S1E) suggest that NAD(H) production is tied with the binding of NADH to enzymes. In particular, lower NAD(H) production is associated with a lower fraction of enzyme-bound NADH (higher  $g$  values), whereas a shift toward higher NAD(H) production is associated with a higher fraction of enzyme-bound NADH (lower  $g$  values). While a strong correspondence between fluorescence lifetimes and NADH activity is observed here, we note that it is possible that other autofluorescent molecules produced by *P. aeruginosa* contribute to the fluorescence lifetime measurements. The results here suggest that NADH is the predominant determinant of fluorescence lifetime in our experiments.

**A growth transition accompanies virulence induction.** We characterized changes in fluorescence lifetime during the onset of virulence. Virulence was measured using an image-based assay using amoebae as host cells (12, 50). This assay is sensitive to virulence-activated and low-virulence phenotypes but does not capture intermediate virulence phenotypes (50). *P. aeruginosa* bacteria that are attached to a rigid substrate transition from a low-virulence state to a virulence-activated state during late exponential phase (12, 13). We confirmed that surface-attached *P. aeruginosa* cells activate virulence in our growth conditions in rich medium using amoebae as host cells and a calcein acetoxymethyl (calcein-AM) stain, which fluoresces when amoebae are stressed (12, 50) (Fig. 3A and B). We also confirmed that surface-activated virulence requires the master quorum-sensing regulator LasR and the surface sensing-associated protein PilY1 (12, 21) (Fig. 3A and B; see also Fig. S3A in the supplemental material). The mutations decrease the density of *P. aeruginosa* on the surface (Fig. S3B). However, we do not attribute the changes in virulence to the decrease in surface density, as the roles of LasR

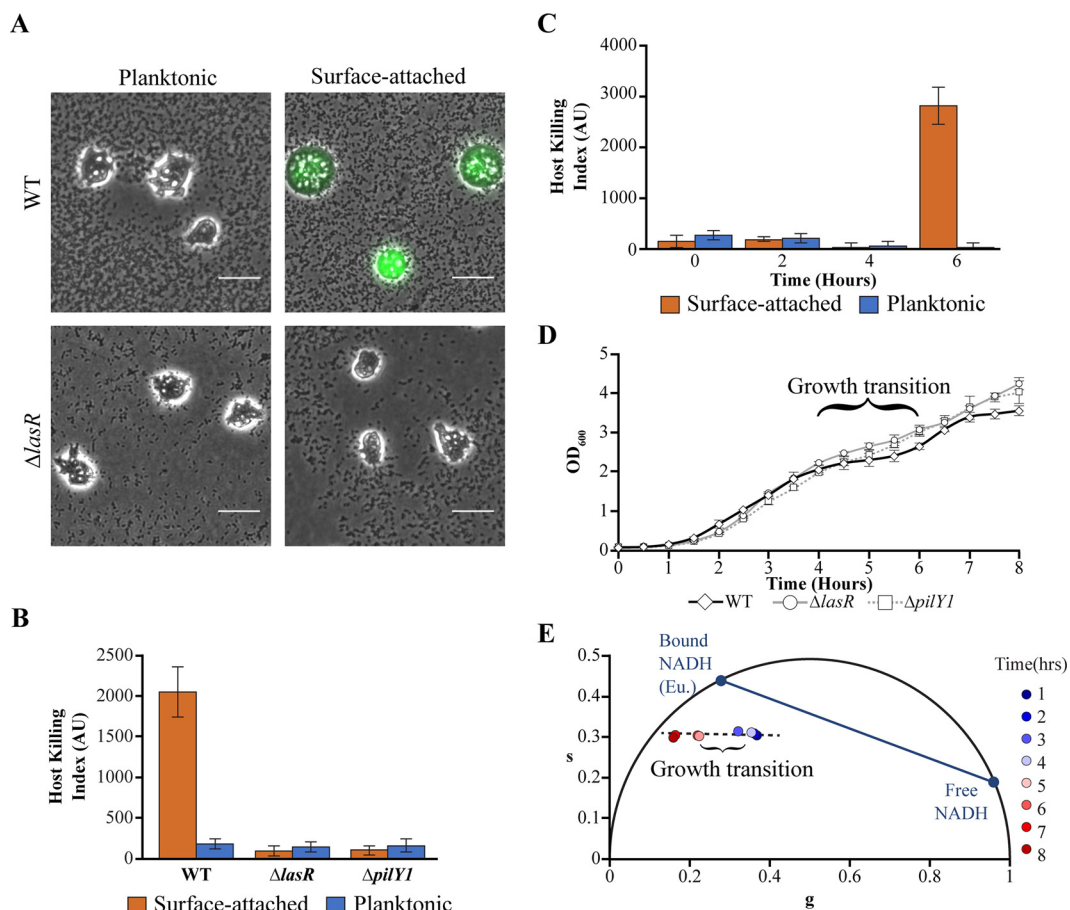


**FIG 3** Virulence activation coincides with a growth transition. (A) An image-based assay using amoeba host cells and calcein-AM fluorescence (green) indicates the virulence of wild-type (WT) *P. aeruginosa* or *P. aeruginosa*  $\Delta LasR$  and is used to compute host killing indexes. Bars, 25  $\mu$ m. (B) Host killing indexes (in arbitrary units [AU]) for planktonic or surface-attached subpopulations of *P. aeruginosa* (wild-type,  $\Delta LasR$ , and  $\Delta pilY1$ ) following 6 h of growth from dilution of a saturated culture. (C) The host killing indexes of planktonic or surface-attached wild-type *P. aeruginosa* following 0, 2, 4, and 6 h of growth. (D and E) Growth profiles measured using optical density (OD<sub>600</sub>) (D) and fluorescence lifetimes of planktonic *P. aeruginosa* (E). For panels B through D, bars and data points represent the average values for three independent experiments, and error bars indicate standard deviations. *P. aeruginosa* were cultured in rich (PS:DB) medium.

and PilY1 in regulating surface-activated virulence have been established previously (12).

To identify the growth period during which virulence is induced, we measured virulence at 2-h intervals following dilution from an overnight saturated culture. Virulence was induced in surface-attached cells during a critical period between 4 to 6 h of growth (Fig. 3C). Interestingly, this critical period was marked by a growth transition that punctuated two distinct periods of exponential growth, as measured by the optical density of planktonic cells from cultures in flasks (Fig. 3D; described in Text S1 in the supplemental material). The growth transition is consistent with a diauxic shift in which the cellular growth rate is temporarily reduced while the enzymes required for utilizing a different metabolic pathway are produced (51). Growth transitions were observed in LasR and PilY1 mutants, which have low virulence, although the transition effects were significantly diminished in these strains (Fig. 3D). To determine whether central metabolic activity is altered during the growth transition, we measured the fluorescence lifetimes of planktonic cells from cultures in flasks. We observed a significant shift in fluorescence lifetimes between 4 and 5 h, coinciding with the growth transition, toward smaller *g* values (Fig. 3E). These results suggest that *P. aeruginosa* undergoes a significant metabolic rearrangement during the virulence induction period.

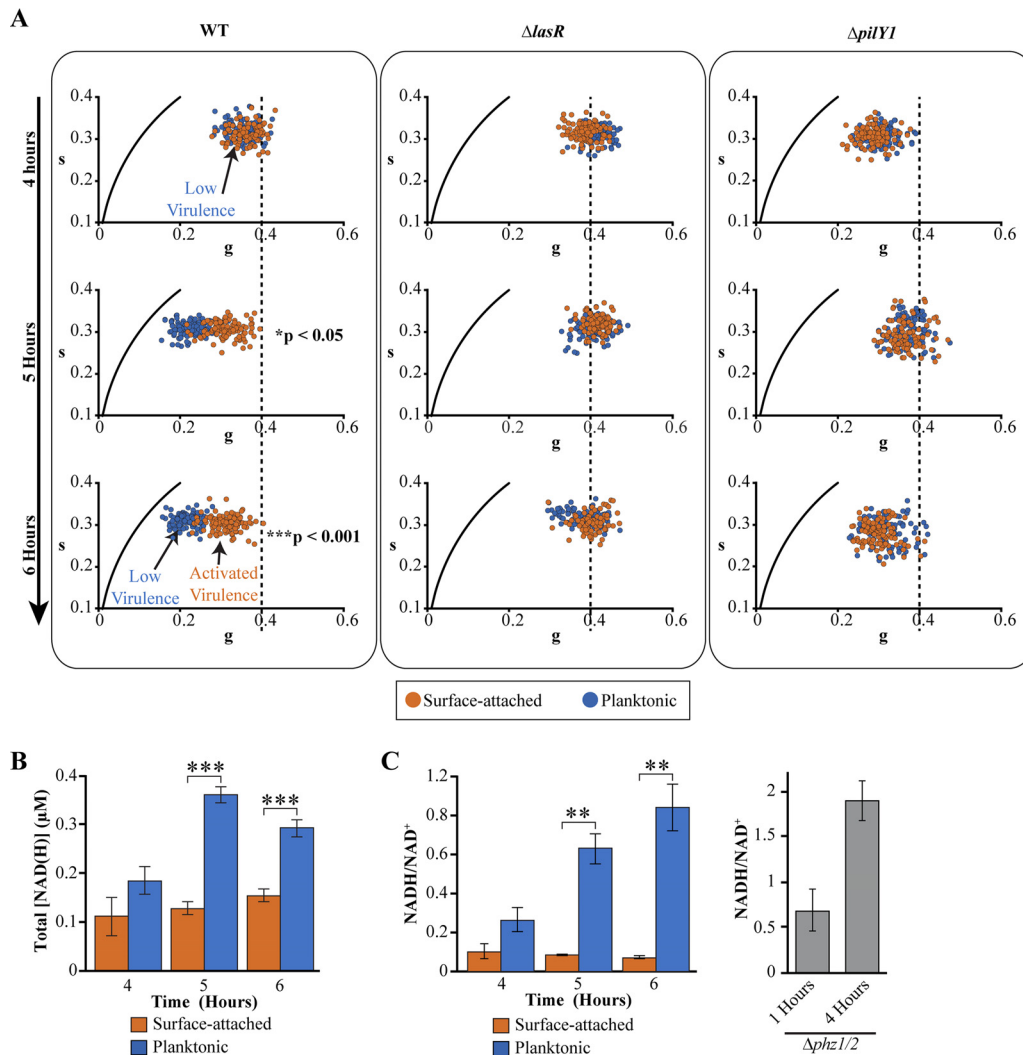


**FIG 4** Virulence-activated and low-virulence populations have distinct fluorescence lifetimes and NAD(H) concentrations. (A) Fluorescence lifetime phasor maps of surface-attached (red) or planktonic (blue) populations of wild-type (left panel),  $\Delta lasR$  (middle panel), or  $\Delta pilY1$  (right panel) *P. aeruginosa* during the growth transition phase. Each data point represents the value for a single *P. aeruginosa* cell. Data are pooled from three independent experiments. A vertical dashed line at a  $g$  value of 0.4 is plotted for reference. (B and C) Total NADH and NAD<sup>+</sup> concentrations (B) and the corresponding NADH/NAD<sup>+</sup> ratios (C) for surface-attached and planktonic wild-type *P. aeruginosa* during the growth transition phase. Bars indicate the mean values from three independent experiments and error bars represent standard deviations. *P. aeruginosa* cells were cultured in rich (PS:DB) medium, with the exception of the  $\Delta phz1/2$  strain, which was cultured in modified MOPS medium. Values that are significantly different are indicated by bars and asterisks as follows: \*\*,  $P < 0.01$ ; \*\*\*,  $P < 0.001$ . Full statistical details are given in Table S1 in the supplemental material.

#### Virulence-activated and low-virulence populations are metabolically distinct.

Planktonic and surface-attached populations develop distinct virulence phenotypes during the growth transition period. At the start of the transition period at 4 h, both populations are in a low-virulence state (Fig. 3C and D). By the end of the transition period, surface-attached cells are induced for virulence, whereas planktonic cells remain in the low-virulence state (Fig. 3C and D). We hypothesized that planktonic and surface-attached cells undergo distinct metabolic changes during the growth transition period.

We monitored the fluorescence lifetimes and NAD(H) production in both populations from the same culture during the growth transition between 4 and 6 h. At the start of the growth transition (4 h following inoculation), the fluorescence lifetime profiles of the two populations were indistinguishable and had comparable  $g$  values (Fig. 4A, top left; see also Fig. S3C in the supplemental material). Two hours following



entry into the growth transition (6 h following inoculation), in which *P. aeruginosa* enters a new period of exponential growth (Fig. 3D), the two populations exhibited distinct metabolic profiles (Fig. 4A, bottom left, and Fig. S3C). Surface-attached cells shifted to a smaller  $g$  value of 0.3, whereas planktonic cells shifted toward a significantly smaller  $g$  value of 0.2 (Fig. 4A, bottom left, and Fig. S3C). Measurements using the enzyme-cycling assay indicated that the subpopulations produced distinct concentrations of NAD(H) after 2 h (Fig. 4B), with the surface-attached population producing significantly lower levels of total NAD(H). This effect was due primarily to lower levels of NADH in the surface-attached population (Fig. S3D and E). Consequently, the NADH/NAD<sup>+</sup> ratios in surface-attached *P. aeruginosa* were significantly lower than those in the planktonic population (Fig. 4C).

These results indicate that surface-attached and planktonic populations have distinct  $g$  values, total NAD(H) concentrations, and NADH/NAD<sup>+</sup> ratios toward the end of the growth transition. In surface-attached *P. aeruginosa*, the decreased NAD(H) production, lower NADH/NAD<sup>+</sup> ratios, and greater abundance of free NADH, as indicated by the FLIM measurements, are consistent with a less active metabolic state compared to the planktonic population. These results suggest that planktonic and surface-attached *P. aeruginosa* enter the growth transition period with identical metabolic states but exit the period with distinct metabolic activities, with the planktonic population having greater NADH-associated metabolic activity than the surface-attached population.

Surface-attached and planktonic cells have distinct host-killing activities at the end of the growth transition, with surface-attached and planktonic cells exhibiting virulence-activated or low-virulence states, respectively (Fig. 3C). Coupled with the observation that surface-attached and planktonic populations have distinct metabolic states, these observations suggest a link between metabolic states and virulence (Fig. 4A). We investigated whether metabolic activity is altered in LasR and PilY1 mutants, which have significantly reduced host-killing activity (12, 15, 16, 19–21). Surface-attached or planktonic populations of these mutants do not kill amoebae (Fig. 3A and B; see also Fig. S3A in the supplemental material). We found that the FLIM  $g$  values of both surface-attached and planktonic populations of these mutants were indistinguishable during the growth transition (Fig. 4A). In particular, we note the higher baseline  $g$  value of 0.4 in the LasR mutant, which suggests a higher abundance of free NADH in this strain. The LasR mutant is impaired in the production of the pyocyanin (52), which functions as a major electron acceptor and reacts with NADH (46). The shift to a higher  $g$  value in the LasR mutant may reflect a lack of interaction between NADH and pyocyanin.

**Perturbation of central metabolism alters virulence activation.** We investigated the extent that altered central metabolic activity affects host-killing activity in surface-attached cells. We cultured *P. aeruginosa* in rich medium and supplemented the cultures at the beginning of growth transition with carbon sources that mapped to distinct positions along the fluorescence lifetime trajectory (Fig. 2E) and that produced distinct changes in NAD(H) production (Fig. 2C). We observed that all carbon sources increased the FLIM  $g$  values, decreased NAD(H) production, and increased NADH/NAD<sup>+</sup> ratios (Fig. 5A to C). The changes in NAD(H) production and NADH/NAD<sup>+</sup> ratios were due primarily to decreases in NAD<sup>+</sup> production (see Fig. S4A in the supplemental material). No change in NADH production was detected. Citrate, and pyruvate produced the greatest increases in  $g$  values, consistent with significant decreases in the relative abundance of enzyme-bound NADH, caused the greatest decreases in NAD(H) production, and caused the greatest increases in NADH/NAD<sup>+</sup> ratio (Fig. 5A to C). In contrast, supplementation with glucose induced relatively small changes in FLIM  $g$  values, NAD(H) production, and NADH/NAD<sup>+</sup> ratios (Fig. 5A to C). These results suggest that the treatment of surface-attached *P. aeruginosa* with carbon sources at the beginning of the growth transition induces the populations into metabolic states that have different levels of NADH activity.

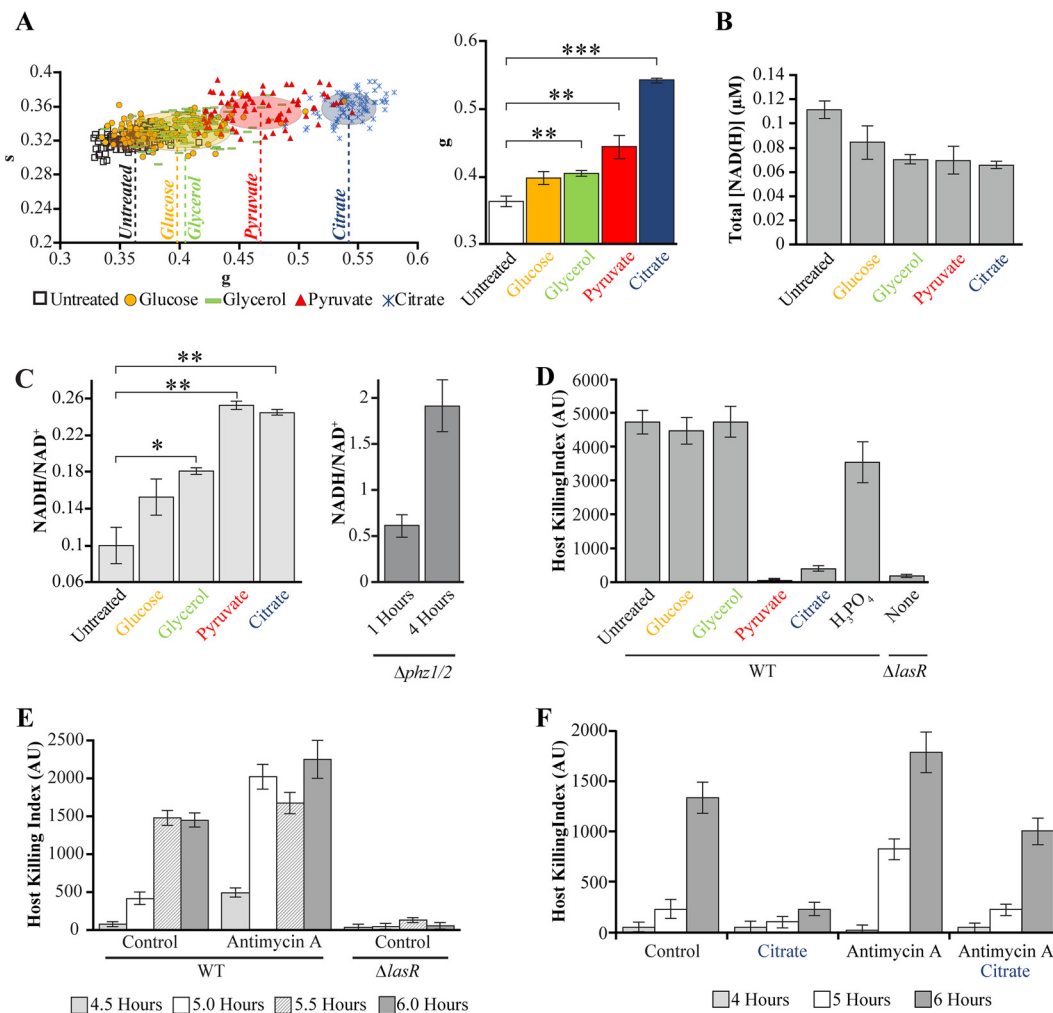


**FIG 5** Perturbing central metabolism inhibits or induces earlier activation of virulence. (A) Fluorescence lifetime phasor plot (left) and  $g$  values (right) of surface-attached *P. aeruginosa* cultured in rich (PS:DB) medium, supplemented with carbon sources at 0.2% concentration at 3 h following dilution, and harvested after an additional hour of growth. Each data point represents the value for a single *P. aeruginosa* cell. The center and axis length of each ellipse corresponds to the mean and standard deviation, respectively, of all cells pooled from three independent experiments. The bars and error bars in the bar graph indicate the means and standard errors of the means of three independent experiments, respectively. (B and C) Total NADH and NAD<sup>+</sup> concentrations (B) and corresponding NADH/NAD<sup>+</sup> ratios (C) for surface-attached *P. aeruginosa* cultured under conditions identical to those in panel A. (D) Host killing indexes for surface-attached wild-type or  $\Delta lasR$  *P. aeruginosa* assessed after 6 h of growth. Wild-type cultures were supplemented after 3 h of growth with individual carbon sources or phosphoric acid, at 0.2% concentration. Bars are the averages for three independent experiments, and error bars represent standard deviations. (E) Host killing indexes of wild-type or  $\Delta lasR$  surface-attached *P. aeruginosa* at 4.5 to 6 h of growth following treatment at 3 h with 0.1% ethanol (control) or 10  $\mu\text{M}$  antimycin A dissolved in 0.1% ethanol. (F) Host killing indexes of wild-type surface-attached *P. aeruginosa* following treatment at 3 h with 0.1% ethanol (control), 0.2% citrate, 10  $\mu\text{M}$  antimycin A dissolved in 0.1% ethanol, or with 0.2% citrate and 10  $\mu\text{M}$  antimycin A dissolved in 0.1% ethanol. All *P. aeruginosa* cells were cultured in rich (PS:DB) medium. Values that are significantly different are indicated by bars and asterisks as follows: \*,  $P < 0.05$ ; \*\*,  $P < 0.01$ ; \*\*\*,  $P < 0.001$ . Full statistical details are given in Table S1 in the supplemental material.

Analysis of host-killing activity revealed that citrate inhibited virulence in surface-attached *P. aeruginosa* (Fig. 5D). Similar results were observed using pyruvate, which had similar impacts on FLIM  $g$  values, NAD(H) production, and NADH/NAD<sup>+</sup> ratios as citrate (Fig. 5A to C). In contrast, treatment with glucose or glycerol, which produced the smallest changes in NADH/NAD<sup>+</sup> ratios and FLIM  $g$  values, had no effect on host-killing activity. The reduction in host-killing activity by citrate or pyruvate was not due to changes in the density of *P. aeruginosa* on surfaces, as the treatments did not decrease the surface density (see Fig. S4B in the supplemental material). The reduction in host-killing activity was also not due to changes in pH, as treatment with phosphoric acid at the same concentration had little impact on host-killing activity (Fig. 5D). These

results suggest that a change in NAD(H) activity and enzyme-bound NADH fraction inhibits the activation of host-killing factors.

In separate experiments, we supplemented cultures at the beginning of the growth transition with antimycin A, which inhibits NADH oxidation. Treatment of surface-attached *P. aeruginosa* with antimycin A induced virulence 30 min earlier than untreated cells (Fig. 5E). This effect was inhibited by the cotreatment of antimycin A with citrate (Fig. 5F).

## DISCUSSION

Bacterial virulence is regulated by a number of factors that ensure successful infection. How the metabolic state of the cell changes during virulence induction has been unknown. Our results indicate that a shift in central metabolism, in the form of changes in NADH and NAD<sup>+</sup> abundances and NADH binding to enzymes, accompanies the induction of virulence in *P. aeruginosa*. Using this finding, we perturb central metabolism to inhibit virulence or to induce virulence at an earlier time. As NADH is utilized as a central metabolic currency broadly across bacterial species, our results suggesting a role for NADH abundance in the regulation of virulence could have far-reaching significance.

We have established a metabolic trajectory in *P. aeruginosa* using the phasor approach to fluorescence lifetime imaging microscopy. We observed that positions along the *g* axis of the fluorescence lifetime trajectory negatively correlated with total NAD(H) production. Greater FLIM *g* values, indicating decreased enzyme-bound NADH within the cell, correlated with decreases in NAD(H) production. In addition, analysis of the cumulative fluorescence lifetime data using a K-means entropy clustering algorithm identified five distinct metabolic states into which *P. aeruginosa* cells can be clustered (see Fig. S5 in the supplemental material).

By establishing fluorescence lifetime maps and performing NAD(H) concentration measurements and host-killing assays, we have measured the dynamics of central metabolism in *P. aeruginosa* during the activation of virulence. Our analysis revealed that *P. aeruginosa* undergoes a rapid and distinct metabolic rearrangement during the growth transition that differentiates cells into low-virulence or virulence-activated populations. At the beginning of the growth transition when *P. aeruginosa* entered a period of reduced growth rate, both planktonic and surface-attached populations were metabolically indistinguishable by FLIM and NAD(H) measurements. At the end of the transition, planktonic populations had an increased proportion of enzyme-bound NADH and increased the production of NAD(H) but did not activate host-killing factors. In contrast, surface-attached populations had comparatively less enzyme-bound NADH and decreased NAD(H) production, which resembled a state of metabolic dormancy, and transitioned to an activated virulence state.

The observation that virulent (surface-attached) populations are metabolically distinct from low-virulence (planktonic) populations raises the possibility that altering central metabolism activity could affect virulence activation. Treatment of surface-attached *P. aeruginosa* with citrate and pyruvate decreased the enzyme-bound NADH pool, decreased the total NAD(H) production, and abolished host-killing activity. In contrast, glucose and glycerol had relatively small impacts on the level of enzyme-bound NADH and NAD(H) production and had no effect on host-killing activity.

The impacts of individual carbon sources on host-killing activity may be interpreted in the context of the glyoxylate pathway, which bypasses the TCA cycle in favor of carbon preservation for gluconeogenesis and biomass production. The glyoxylate pathway activates the expression of type III secretion system and is important for lung infection models (53, 54). Growth in citrate and pyruvate in *P. aeruginosa* biases metabolic activity in favor of the TCA pathway and away from the glyoxylate pathway (55). Thus, the inhibition of virulence observed here could be explained by the inhibition of the glyoxylate pathway by citrate or pyruvate. Treatment of surface-attached *P. aeruginosa* using an oxidase inhibitor induced virulence at an earlier time, which was also inhibited by treatment of citrate. Glucose does not appear to inhibit the

glyoxylate pathway, and glycerol is not expected to inhibit the pathway (55). Consistent with our interpretation, supplementation with glucose or glycerol had no impact on host-killing activity. Together, our results suggest a model in which the glyoxylate pathway is activated in surface-attached populations, which results in the expression of host-killing factors. In this model, the activation of the pathway can be inhibited by citrate or pyruvate, but not by glucose or glycerol. The observed changes in NAD(H) production and the fraction of enzyme-bound NADH may be indicative of changes in TCA and glyoxylate pathway utilization. The decreased production of NAD(H) in surface-attached populations is consistent with inactivation of the TCA cycle in favor of the glyoxylate pathway.

A recent preprint indicates that alkyl quinolines are responsible for cytotoxicity in surface-associated populations (16). Anthranilate is a metabolic precursor for quinolones (56), and its availability may have a significant impact on the production of these cytotoxic factors in surface-associated populations. The alteration of central metabolites could thus function as a regulator to rapidly coordinate virulence during the critical growth transition period.

Virulence is observed in our experiments only in surface-attached cells. Low-virulence planktonic cells produce greater levels of NAD(H) and have greater enzyme-bound NADH. The mechanisms that give rise to the distinct metabolic states are unclear. The availability of electron acceptors and surface sensing in *P. aeruginosa* could have an impact on metabolism. These results thus suggest an important role for electron transfer activity in the activation of virulence mechanisms. Future experiments will need to address the extent to which NAD(H) production and free NADH in planktonic cells impact the production of host-killing factors.

Fluorescence lifetime imaging microscopy provides spatial measurements of metabolism and may be a useful tool for measuring metabolic activity across multiple length scales from single cells to mature biofilms. We observed that fluorescence lifetimes were spatially heterogeneous in the cytoplasm of *P. aeruginosa*, which is consistent with the subcellular localization of metabolic activity (57). Future experiments will need to address the impact of changes in central metabolism on the spatial organization of NADH activity. In addition, metabolic dormancy in biofilms is associated with antibiotic resistance (58). The use of FLIM to map spatial changes in metabolism in biofilms may thus open new avenues for the investigation of antibiotic resistance in biofilms.

Antivirulence therapy is a proposed strategy for combating pathogenesis as an alternative to conventional antibiotics, which typically target bacterial growth (59). The identification that NADH levels affect virulence induction highlights a potential target for virulence inhibition. Our results suggest metabolic manipulation as a strategy to inhibit virulence. Strategies such as targeting metabolic pathways involved in NAD(H) production or growth in the presence of bacteria that secrete metabolites that affect NAD(H) production could be effective at inhibiting virulence. Within microbiomes, complex microbial communities, and host environments, metabolite cross-feeding could have a significant impact on virulence activation in pathogens.

## MATERIALS AND METHODS

**Growth conditions and strains.** *Pseudomonas aeruginosa* strains were streaked onto LB-Miller (BD Biosciences, Franklin Lakes, NJ) petri dishes containing 2% Bacto agar (BD Biosciences) and incubated at 37°C to obtain single colonies. Individual colonies were inoculated into modified PS:DB, which is a rich medium that supports coculturing of *P. aeruginosa* cells with *Dictyostelium discoideum* (amoeba) (12). The modified PS:DB medium, hereafter referred to as PS:DB medium in this work, is the same formulation of PS:DB medium as described previously (12) except that PS medium was used at a concentration of 90% (vol/vol) instead of 10% (vol/vol). *P. aeruginosa* strains were cultured overnight in PS:DB medium in a rotary drum rotating at 24 rpm or orbital shaker rotating at 200 rpm and 37°C, diluted 1:100 into a plastic or glass dish containing the same medium, and cultured between 4 to 6 h. Alternatively, strains were cultured in minimal medium A (60) containing 0.2% glucose, diluted 1:100 into minimal medium A that was modified to exclude citrate (hereafter referred to as modified minimal medium A) and containing one of the following carbon sources at a concentration of 0.2%: glucose, glycerol, citrate, or pyruvate (Sigma, St. Louis, MO), and cultured to an optical density at 600 nm ( $OD_{600}$ ) of 0.2 at 37°C.

*D. discoideum* was grown axenically in PS medium at 22°C as described previously (12) and harvested for virulence assays when cultures reached an OD<sub>600</sub> between 0.2 to 0.5.

Wild-type *P. aeruginosa* strain PA14 (61), PA14 strains containing a  $\Delta lasR$  (AFS20.1) (62) or  $\Delta pilY1$  (19) deletion, a  $pvdA::Mar2xT7$  mutation (63), or the  $\Delta phzA1-G1 \Delta phzA2-G2$  mutations (64, 65) (original strain name DKN330, referred to here as  $\Delta phz1/2$ ), and the *D. discoideum* strain AX3 (66) were used for these experiments.

**Fluorescence lifetime imaging microscopy (FLIM).** Fluorescence lifetime measurements were performed using a custom-built multiphoton microscope setup based on an Olympus FV1000 system and an Olympus IX81 microscope (Olympus, Waltham, Massachusetts) as described previously (67). The FLIM microscope uses an 80 MHz ultrafast Ti:Sapphire Mai Tai laser (Spectra-Physics, Santa Clara, CA) set at 740 nm for multiphoton excitation. The setup used a 690-nm SP dichroic 460/80-nm filter pair for separating emission and a PlanApo N Olympus oil immersion 60× (1.42-numerical-aperture [NA]) objective (Olympus, Waltham, MA), which is capable of bacterial single-cell resolution imaging. An H7422P-40 photomultiplier tube module (Hamamatsu, Bridgewater, NJ) and A320 FastFLIM Box (ISS, Champaign, IL) were used to measure fluorescence lifetime. Image acquisition was controlled by SimFCS software version 4 (64-bit) (Laboratory for Fluorescence Dynamics, Irvine, CA). Planktonic and surface-attached cells were isolated by modifying a protocol described previously (12, 50) (see Fig. S6A in the supplemental material).

Masks for bacterial cells were created through SimFCS using fluorescence intensity images and image intensity thresholding (see Fig. S6B in the supplemental material). Fluorescence lifetimes within the masked areas were transformed using  $g_{ij}(\omega) = \int_0^\infty I_{ij}(t) \cos(\omega t) dt / \int_0^\infty I_{ij}(t) dt$  and  $s_{ij}(\omega) = \int_0^\infty I_{ij}(t) \sin(\omega t) dt / \int_0^\infty I_{ij}(t) dt$ , where  $I(t)$  is the fluorescence intensity decay,  $\omega$  is the laser repetition angular frequency, and the indexes  $i$  and  $j$  identify a pixel of the image.

The microscope was calibrated before each session by setting the fluorescence lifetime obtained for 10  $\mu$ M rhodamine 110 (Sigma, St. Louis, MO) to 4.0 ns. The laser power was set at 20% (<3 mW at the back aperture of the microscope) using an acousto-optic modulator (AA Opto Electronic, Orsay, France). Subcellular fluorescence lifetimes (Fig. 1A) were collected using the 20× digital zoom mode at a rate of 1.7 s/frame. All other *P. aeruginosa* measurements were performed using the 6× digital zoom mode using the same frame rate. For all measurements, 40 sequential frames were acquired to generate a single FLIM image.

**Virulence assay.** *P. aeruginosa* cells were assayed using an image-based virulence assay as described previously (12, 50). *P. aeruginosa* strains were cultured in PS:DB medium, diluted 1:100 into plastic petri dishes (60 by 15 mm) (Corning, Corning, NY), cultured for 4 to 6 h by shaking at 100 rpm, and harvested. Planktonic cells were assayed by transferring 10- $\mu$ l volume of culture from the petri dish to a new petri dish, mixing with an equal volume of *D. discoideum* that had been grown to an OD<sub>600</sub> of 0.2 to 0.5, and immobilizing by placing an agar pad on top of the mixture (see Fig. S6C in the supplemental material). Agar pads were made using Bacto agar at a concentration of 1%, DB buffer, and 1  $\mu$ M calcein acetoxymethyl (calcein-AM) ester (Molecular Probes, Eugene, OR) and were cut into 1.5- by 1.5-cm squares (12, 50). Surface-attached cells were assayed by aspirating planktonic cells from the culture, washing with DB buffer to remove planktonic cells, mixing with an equal volume of *D. discoideum*, and immobilizing by placing an agar pad on top of the mixture (Fig. S6C) (50). The immobilized planktonic or surface-attached *P. aeruginosa* and *D. discoideum* were incubated at room temperature for 1 h and imaged using fluorescence microscopy. The host killing index (12, 50) was computed as the average ratio of calcein-AM fluorescence to cell area in individual amoeba cells for 30 to 200 cells in each experiment.

Fluorescence microscopy to assess calcein-AM fluorescence was performed using a Nikon Eclipse Ti-E microscope (Nikon, Melville, NY) containing Nikon 10× Plan Fluor Ph1 (0.3-NA) and 20× S Plan Fluor Nikon (0.45-NA) objectives, a Sola light engine (Lumencor, Beaverton, OR), an LED-DA/FI/TX filter set (Semrock, Rochester, NY) containing a 409/493/596 dichroic and 474/27-nm and 525/45-nm filters for excitation and emission, respectively, and a Hamamatsu Orca Flash 4.0 V2 camera (Hamamatsu, Bridgewater, NJ). Images were acquired using Nikon NIS-Elements and analyzed using custom-built software written previously (12) in Matlab (Mathworks, Natick, MA).

**NAD (NADH, NAD<sup>+</sup>) concentrations.** The concentrations of reduced and oxidized NAD (NADH, NAD<sup>+</sup>) were measured using a colorimetric enzyme-cycling assay as described previously (45). *P. aeruginosa* strains were cultured overnight in PS:DB medium, diluted 1:100 into plastic petri dishes (60 by 15 mm) (Corning, Corning, NY) containing the same medium, and grown for 4 to 6 h. Alternatively, strains were cultured overnight in minimal medium, diluted 1:100 into plastic petri dishes containing modified minimal medium with single carbon sources, and grown to an OD<sub>600</sub> of 0.2. Cultures were harvested in a glove box chamber (Bel-Art, Wayne, NJ) that had been vacuumed to remove air and flushed with nitrogen constantly throughout the experiment to prevent oxidation of NADH. Subsequent steps were performed, and solutions were prepared in the glove box unless otherwise indicated. Solutions containing 0.05 to 1  $\mu$ M of NADH (Sigma) or NAD<sup>+</sup> (Sigma) were included as calibration controls.

Planktonic cells were isolated from petri dishes and pelleted by centrifugation at 16,000 × *g* for 1 min, the residual supernatant was discarded, and the pellet was immediately resuspended in 0.2 M NaOH or HCl to extract NADH or NAD<sup>+</sup>, respectively, as described previously (45, 46). Surface-attached cells were harvested by aspirating planktonic cells from petri dishes, washing with DB buffer or modified minimal medium with no carbon source for strains cultured in PS:DB medium or modified minimal medium A containing single carbon sources, respectively, adding 0.2 M NaOH or HCl, and scraping surfaces with a cell scraper (Sarstedt, Nümbrecht, Germany). For a control, the  $\Delta phz1/2$  strain was cultured overnight in modified morpholinepropanesulfonic acid (MOPS) synthetic medium (46), diluted 1:100 in the same medium in culture tubes for 1 to 4 h, pelleted by centrifugation, and resuspended in

0.2 M NaOH or HCl, as described previously (46). The resuspensions in NaOH or HCl were neutralized using equal volume of 0.1 M HCl or NaOH, respectively, and portions were assayed for protein content, NADH, and NAD<sup>+</sup>. Resuspensions were assayed for protein content using a BCA assay kit (ThermoFisher Scientific, Waltham, MA) using a 50:1 mixture of solutions A and B from the kit. Solutions were incubated at 37°C for 30 min and measured for absorbance at 562 nm. Resuspensions that were not used for the BCA assay were normalized by protein content by diluting in Millipore filtered water.

NADH and NAD<sup>+</sup> concentrations were determined by following the protocol described previously (45). Briefly, normalized resuspensions were centrifuged at 16,000 × *g* for 10 min at 4°C to remove cell debris and mixed with a reaction mixture containing 40 mM EDTA, 1 M bicine (Sigma), 4.2 mM 3-(4,5-dimethylthiazol-2-yl)-2,5-diphenyltetrazolium bromide (Sigma), 16.6 mM phenazine ethosulfate (Sigma), 1 mg/ml alcohol dehydrogenase (Sigma), and ethanol, and the absorbance at 570 nm of the solution was measured in a 96-well plate (Corning, Corning, NY) at 30°C every 30 s for 30 min using a BioTek Synergy HTX reader (BioTek, Winooski, VT). The reaction mixture and the normalized resuspensions were aliquoted and mixed inside the glove box. The centrifugation and absorbance measurements were performed outside the glove box. The absorbance per unit time was determined by fitting data on the initial velocity of enzyme activity, acquired between 2 and 10 min of the absorbance measurements. The absorbances per unit time for the NADH and NAD<sup>+</sup> calibration controls were linearly fit for the full range of calibration concentrations to establish a linear equation that relates the absorbance per unit time and NAD(H) concentration. The NAD(H) concentrations of the planktonic and surface-attached cell resuspensions were determined by inputting the respective absorbance per unit time fits of the samples into these equations.

**Statistical analysis.** The significance of changes between experimental conditions was determined by using unpaired two-tailed heteroscedastic *t* tests. The *t* values, degrees of freedom, and *P* values are given in Table S1 in the supplemental material. For fluorescence lifetime phasor plots, the center of ellipses indicates the mean of all cells pooled from multiple experiments. The axis lengths of the ellipses indicate the standard deviation of the pooled data set. Unless otherwise indicated, bars and error bars in bar graphs indicate the mean and standard deviation of the means from multiple independent experiments, respectively.

Further details on growth conditions, measurements of growth profiles, FLIM measurements, surface density measurements, and the classifier model are described in Text S1 in the supplemental material.

## SUPPLEMENTAL MATERIAL

Supplemental material is available online only.

**TEXT S1**, PDF file, 0.1 MB.

**FIG S1**, PDF file, 0.1 MB.

**FIG S2**, PDF file, 0.1 MB.

**FIG S3**, PDF file, 0.1 MB.

**FIG S4**, PDF file, 0.1 MB.

**FIG S5**, PDF file, 1.8 MB.

**FIG S6**, PDF file, 0.2 MB.

**TABLE S1**, PDF file, 0.1 MB.

## ACKNOWLEDGMENTS

We thank members of the UCI Systems Microbiology Group, K. Whiteson, E. Gratton, and A. Hochbaum for helpful input on analysis and interpretation of fluorescence lifetime data, R. Datta for previous fluorescence lifetime measurements of *P. aeruginosa*, and an anonymous reviewer who pointed out the role of the glyoxylate pathway.

This work was supported by a National Institutes of Health (NIH) Career Transition Award (K22AI112816) to A.S., an NIH R21 Award (R21AI139968) to A.S. and M.D., and a UC Irvine Center for Complex Biological Systems Opportunity Award to A.K. and J.V.C. provided by NIH-NIGMS (National Institute of General Medical Sciences) P50-GM076516. The experiments reported in this paper were performed at the Laboratory for Fluorescence Dynamics (LFD) at the University of California, Irvine, which is supported jointly by the National Institutes of Health (2P41GM103540) and UC Irvine.

J.V.C., A.K., A.S., and M.A.D. conceived the project. J.V.C. and K.P. conducted experiments and analyzed data. A.S. and M.A.D. provided overall project direction. K.P., J.V.C., A.S., and M.A.D. designed experiments, discussed the results, and wrote and revised the manuscript.

## REFERENCES

- Driscoll JA, Brody SL, Kollef MH. 2007. The epidemiology, pathogenesis and treatment of *Pseudomonas aeruginosa* infections. *Drugs* 67: 351–368. <https://doi.org/10.2165/00003495-200767030-00003>.
- Lee DG, Urbach JM, Wu G, Liberati NT, Feinbaum RL, Miyata S, Diggins LT, He J, Saucier M, Déziel E, Friedman L, Li L, Grills G, Montgomery K, Kuchlerapati R, Rahme LG, Ausubel FM. 2006. Genomic analysis reveals that *Pseudomonas aeruginosa* virulence is combinatorial. *Genome Biol* 7:R90. <https://doi.org/10.1186/gb-2006-7-10-r90>.
- Rahme LG, Ausubel FM, Cao H, Drenkard E, Goumnerov BC, Lau GW, Mahajan-Miklos S, Plotnikova J, Tan MW, Tsongalis J, Walendziewicz CL, Tompkins RG. 2000. Plants and animals share functionally common bacterial virulence factors. *Proc Natl Acad Sci U S A* 97:8815–8821. <https://doi.org/10.1073/pnas.97.16.8815>.
- Pukatzki S, Kessin RH, Mekalanos JJ. 2002. The human pathogen *Pseudomonas aeruginosa* utilizes conserved virulence pathways to infect the social amoeba *Dictyostelium discoideum*. *Proc Natl Acad Sci U S A* 99:3159–3164. <https://doi.org/10.1073/pnas.052704399>.
- Hauser AR. 2009. The type III secretion system of *Pseudomonas aeruginosa*: infection by injection. *Nat Rev Microbiol* 7:654–665. <https://doi.org/10.1038/nrmicro2199>.
- Van Alst NE, Picardo KF, Iglewski BH, Haidaris CG. 2007. Nitrate sensing and metabolism modulate motility, biofilm formation, and virulence in *Pseudomonas aeruginosa*. *Infect Immun* 75:3780–3790. <https://doi.org/10.1128/IAI.00201-07>.
- Palmer GC, Whiteley M. 2015. Metabolism and pathogenicity of *Pseudomonas aeruginosa* infections in the lungs of individuals with cystic fibrosis. *Microbiol Spectr* 3(4):MBP-0003-2014. <https://doi.org/10.1128/microbiolspec.MBP-0003-2014>.
- Bartell JA, Blazier AS, Yen P, Thøgersen JC, Jelsbak L, Goldberg JB, Papin JA. 2017. Reconstruction of the metabolic network of *Pseudomonas aeruginosa* to interrogate virulence factor synthesis. *Nat Commun* 8:14631. <https://doi.org/10.1038/ncomms14631>.
- Eisenreich W, Dandekar T, Heesemann J, Goebel W. 2010. Carbon metabolism of intracellular bacterial pathogens and possible links to virulence. *Nat Rev Microbiol* 8:401–412. <https://doi.org/10.1038/nrmicro2351>.
- Somerville GA, Proctor RA. 2009. At the crossroads of bacterial metabolism and virulence factor synthesis in staphylococci. *Microbiol Mol Biol Rev* 73:233–248. <https://doi.org/10.1128/MMBR.00005-09>.
- Gode-Potratz CJ, Kustusch RJ, Breheny PJ, Weiss DS, McCarter LL. 2011. Surface sensing in *Vibrio parahaemolyticus* triggers a programme of gene expression that promotes colonization and virulence: surface-responsive gene expression. *Mol Microbiol* 79:240–263. <https://doi.org/10.1111/j.1365-2958.2010.07445.x>.
- Siryaporn A, Kuchma SL, O'Toole GA, Gitai Z. 2014. Surface attachment induces *Pseudomonas aeruginosa* virulence. *Proc Natl Acad Sci U S A* 111:16860–16865. <https://doi.org/10.1073/pnas.1415712111>.
- Persat A, Inclan YF, Engel JN, Stone HA, Gitai Z. 2015. Type IV pili mechanochemically regulate virulence factors in *Pseudomonas aeruginosa*. *Proc Natl Acad Sci U S A* 112:7563–7568. <https://doi.org/10.1073/pnas.1502025112>.
- Alsharif G, Ahmad S, Islam MS, Shah R, Busby SJ, Krachler AM. 2015. Host attachment and fluid shear are integrated into a mechanical signal regulating virulence in *Escherichia coli* O157:H7. *Proc Natl Acad Sci U S A* 112:5503–5508. <https://doi.org/10.1073/pnas.1422986112>.
- Chuang SK, Vrla GD, Fröhlich KS, Gitai Z. 2019. Surface association sensitizes *Pseudomonas aeruginosa* to quorum sensing. *Nat Commun* 10:4118. <https://doi.org/10.1038/s41467-019-12153-1>.
- Vrla GD, Esposito M, Zhang C, Kang Y, Seyedsayamdost MR, Gitai Z. 2020. Surface association induces cytotoxic alkyl-quinolones in *Pseudomonas aeruginosa*. *bioRxiv*. <https://doi.org/10.1101/773291>.
- Bohn Y-S, Brandes G, Rakhimova E, Horatzek S, Salunkhe P, Munder A, van Barneveld A, Jordan D, Bredenbruch F, Häussler S, Riedel K, Eberl L, Jensen PØ, Bjarnsholt T, Moser C, Hoiby N, Tümmler B, Wiehlmann L. 2009. Multiple roles of *Pseudomonas aeruginosa* TBCF10839 PiiY1 in motility, transport and infection. *Mol Microbiol* 71:730–747. <https://doi.org/10.1111/j.1365-2958.2008.06559.x>.
- Heiniger RW, Winther-Larsen HC, Pickles RJ, Koomey M, Wolfgang MC. 2010. Infection of human mucosal tissue by *Pseudomonas aeruginosa* requires sequential and mutually dependent virulence factors and a novel pilus-associated adhesin: factors involved in *P. aeruginosa* tissue infection. *Cell Microbiol* 12:1158–1173. <https://doi.org/10.1111/j.1462-5822.2010.01461.x>.
- Kuchma SL, Ballok AE, Merritt JH, Hammond JH, Lu W, Rabinowitz JD, O'Toole GA. 2010. Cyclic-di-GMP-mediated repression of swarming motility by *Pseudomonas aeruginosa*: the pilY1 gene and its impact on surface-associated behaviors. *J Bacteriol* 192:2950–2964. <https://doi.org/10.1128/JB.01642-09>.
- Rodesney CA, Roman B, Dhamani N, Cooley BJ, Katira P, Touhami A, Gordon VD. 2017. Mechanosensing of shear by *Pseudomonas aeruginosa* leads to increased levels of the cyclic-di-GMP signal initiating biofilm development. *Proc Natl Acad Sci U S A* 114:5906–5911. <https://doi.org/10.1073/pnas.1703255114>.
- Luo Y, Zhao K, Baker AE, Kuchma SL, Coggan KA, Wolfgang MC, Wong GCL, O'Toole GA. 2015. A hierarchical cascade of second messengers regulates *Pseudomonas aeruginosa* surface behaviors. *mBio* 6:e02456-14. <https://doi.org/10.1128/mBio.02456-14>.
- Pesci EC, Pearson JP, Seed PC, Iglewski BH. 1997. Regulation of las and rhl quorum sensing in *Pseudomonas aeruginosa*. *J Bacteriol* 179: 3127–3132. <https://doi.org/10.1128/jb.179.10.3127-3132.1997>.
- Miller MB, Bassler BL. 2001. Quorum sensing in bacteria. *Annu Rev Microbiol* 55:165–199. <https://doi.org/10.1146/annurev.micro.55.1.165>.
- O'Connor JR, Kuwada NJ, Huangyuthitham V, Wiggins PA, Harwood CS. 2012. Surface sensing and lateral subcellular localization of WspA, the receptor in a chemosensory-like system leading to c-di-GMP production: WspA functional domains. *Mol Microbiol* 86:720–729. <https://doi.org/10.1111/mmi.12013>.
- Davenport PW, Griffin JL, Welch M. 2015. Quorum sensing is accompanied by global metabolic changes in the opportunistic human pathogen *Pseudomonas aeruginosa*. *J Bacteriol* 197:2072–2082. <https://doi.org/10.1128/JB.02557-14>.
- Clayton AHA, Hanley QS, Verveer PJ. 2004. Graphical representation and multicomponent analysis of single-frequency fluorescence lifetime imaging microscopy data. *J Microsc* 213:1–5. <https://doi.org/10.1111/j.1365-2818.2004.01265.x>.
- Digman MA, Caiolfa VR, Zamai M, Gratton E. 2008. The phasor approach to fluorescence lifetime imaging analysis. *Biophys J* 94:L14–L16. <https://doi.org/10.1529/biophysj.107.120154>.
- Stringari C, Edwards RA, Pate KT, Waterman ML, Donovan PJ, Gratton E. 2012. Metabolic trajectory of cellular differentiation in small intestine by phasor fluorescence lifetime microscopy of NADH. *Sci Rep* 2:568. <https://doi.org/10.1038/srep00568>.
- Wright BK, Andrews LM, Markham J, Jones MR, Stringari C, Digman MA, Gratton E. 2012. NADH distribution in live progenitor stem cells by phasor-fluorescence lifetime image microscopy. *Biophys J* 103:L7–L9. <https://doi.org/10.1016/j.bpj.2012.05.038>.
- Stringari C, Nourse JL, Flanagan LA, Gratton E. 2012. Phasor fluorescence lifetime microscopy of free and protein-bound NADH reveals neural stem cell differentiation potential. *PLoS One* 7:e48014. <https://doi.org/10.1371/journal.pone.0048014>.
- Quinn KP, Sridharan GV, Hayden RS, Kaplan DL, Lee K, Georgakoudi I. 2013. Quantitative metabolic imaging using endogenous fluorescence to detect stem cell differentiation. *Sci Rep* 3:3432. <https://doi.org/10.1038/srep03432>.
- Stringari C, Wang H, Geyfman M, Crosignani V, Kumar V, Takahashi JS, Andersen B, Gratton E. 2015. In vivo single-cell detection of metabolic oscillations in stem cells. *Cell Rep* 10:1–7. <https://doi.org/10.1016/j.celrep.2014.12.007>.
- Jakobs S, Subramaniam V, Schönle A, Jovin TM, Hell SW. 2000. EGFP and DsRed expressing cultures of *Escherichia coli* imaged by confocal, two-photon and fluorescence lifetime microscopy. *FEBS Lett* 479:131–135. [https://doi.org/10.1016/s0014-5793\(00\)01896-2](https://doi.org/10.1016/s0014-5793(00)01896-2).
- Micic M, Hu D, Suh YD, Newton G, Romine M, Lu HP. 2004. Correlated atomic force microscopy and fluorescence lifetime imaging of live bacterial cells. *Colloids Surf B Biointerfaces* 34:205–212. <https://doi.org/10.1016/j.colsurfb.2003.10.020>.
- Gee ML, Burton M, Grevis-James A, Hossain MA, McArthur S, Palombo EA, Wade JD, Clayton A. 2013. Imaging the action of antimicrobial peptides on living bacterial cells. *Sci Rep* 3:1557. <https://doi.org/10.1038/srep01557>.
- Torno K, Wright BK, Jones MR, Digman MA, Gratton E, Phillips M. 2013. Real-time analysis of metabolic activity within *Lactobacillus acidophilus*

- by phasor fluorescence lifetime imaging microscopy of NADH. *Curr Microbiol* 66:365–367. <https://doi.org/10.1007/s00284-012-0285-2>.
37. Bhattacharjee A, Datta R, Gratton E, Hochbaum AI. 2017. Metabolic fingerprinting of bacteria by fluorescence lifetime imaging microscopy. *Sci Rep* 7:3743. <https://doi.org/10.1038/s41598-017-04032-w>.
  38. Bird DK, Yan L, Vrotsos KM, Eliceiri KW, Vaughan EM, Keely PJ, White JG, Ramanujam N. 2005. Metabolic mapping of MCF10A human breast cells via multiphoton fluorescence lifetime imaging of the coenzyme NADH. *Cancer Res* 65:8766–8773. <https://doi.org/10.1158/0008-5472.CAN-04-3922>.
  39. Stringari C, Cinquin A, Cinquin O, Digman MA, Donovan PJ, Gratton E. 2011. Phasor approach to fluorescence lifetime microscopy distinguishes different metabolic states of germ cells in a live tissue. *Proc Natl Acad Sci U S A* 108:13582–13587. <https://doi.org/10.1073/pnas.1108161108>.
  40. Wright BK, Andrews LM, Jones MR, Stringari C, Digman MA, Gratton E. 2012. Phasor-flim analysis of NADH distribution and localization in the nucleus of live progenitor myoblast cells. *Microsc Res Tech* 75:1717–1722. <https://doi.org/10.1002/jemt.22121>.
  41. Mayevsky A, Rogatsky GG. 2007. Mitochondrial function in vivo evaluated by NADH fluorescence: from animal models to human studies. *Am J Physiol Cell Physiol* 292:C615–C640. <https://doi.org/10.1152/ajpcell.00249.2006>.
  42. Lessie TG, Phibbs PV. 1984. Alternative pathways of carbohydrate utilization in pseudomonads. *Annu Rev Microbiol* 38:359–388. <https://doi.org/10.1146/annurev.mi.38.100184.002043>.
  43. Conway T. 1992. The Entner-Doudoroff pathway: history, physiology and molecular biology. *FEMS Microbiol Rev* 9:1–28. <https://doi.org/10.1111/j.1574-6968.1992.tb05822.x>.
  44. Williams HD, Zlosnik JEA, Ryall B. 2006. Oxygen, cyanide and energy generation in the cystic fibrosis pathogen *Pseudomonas aeruginosa*. *Adv Microb Physiol* 52:1–71. [https://doi.org/10.1016/S0065-2911\(06\)52001-6](https://doi.org/10.1016/S0065-2911(06)52001-6).
  45. Kern SE, Price-Whelan A, Newman DK. 2014. Extraction and measurement of NAD(P)<sup>+</sup> and NAD(P)H. *Methods Mol Biol* 1149:311–323. [https://doi.org/10.1007/978-1-4939-0473-0\\_26](https://doi.org/10.1007/978-1-4939-0473-0_26).
  46. Price-Whelan A, Dietrich LEP, Newman DK. 2007. Pyocyanin alters redox homeostasis and carbon flux through central metabolic pathways in *Pseudomonas aeruginosa* PA14. *J Bacteriol* 189:6372–6381. <https://doi.org/10.1128/JB.00505-07>.
  47. Meyer J-M. 2000. Pyoverdines: pigments, siderophores and potential taxonomic markers of fluorescent *Pseudomonas* species. *Arch Microbiol* 174:135–142. <https://doi.org/10.1007/s002030000188>.
  48. Matsushita K, Yamada M, Shinagawa E, Adachi O, Ameyama M. 1980. Membrane-bound respiratory chain of *Pseudomonas aeruginosa* grown aerobically. *J Bacteriol* 141:389–392. <https://doi.org/10.1128/JB.141.1.389-392.1980>.
  49. Shvinka JE, Toma MK, Galinina NI, Skards IV, Viesturs UE. 1979. Production of superoxide radicals during bacterial respiration. *J Gen Microbiol* 113:377–382. <https://doi.org/10.1099/00221287-113-2-377>.
  50. Perinbam K, Siryaporn A. 2018. A rapid image-based bacterial virulence assay using amoeba. *J Vis Exp* 2018:57844. <https://doi.org/10.3791/57844>.
  51. Monod J. 1949. The growth of bacterial cultures. *Annu Rev Microbiol* 3:371–394. <https://doi.org/10.1146/annurev.mi.03.100149.002103>.
  52. Lau GW, Hassett DJ, Ran H, Kong F. 2004. The role of pyocyanin in *Pseudomonas aeruginosa* infection. *Trends Mol Med* 10:599–606. <https://doi.org/10.1016/j.molmed.2004.10.002>.
  53. Lindsey TL, Hagins JM, Sokol PA, Silo-Suh LA. 2008. Virulence determinants from a cystic fibrosis isolate of *Pseudomonas aeruginosa* include isocitrate lyase. *Microbiology* 154:1616–1627. <https://doi.org/10.1099/mic.0.2007/014506-0>.
  54. Chung JCS, Rzhepishevskaya O, Ramstedt M, Welch M. 2013. Type III secretion system expression in oxygen-limited *Pseudomonas aeruginosa* cultures is stimulated by isocitrate lyase activity. *Open Biol* 3:120131. <https://doi.org/10.1098/rsob.120131>.
  55. Crousilles A, Dolan SK, Brear P, Chirgadze DY, Welch M. 2018. Gluconeogenic precursor availability regulates flux through the glyoxylate shunt in *Pseudomonas aeruginosa*. *J Biol Chem* 293:14260–14269. <https://doi.org/10.1074/jbc.RA118.004514>.
  56. Farrow JM, Pesci EC. 2007. Two distinct pathways supply anthranilate as a precursor of the *Pseudomonas* quinolone signal. *J Bacteriol* 189:3425–3433. <https://doi.org/10.1128/JB.00209-07>.
  57. Ingerson-Mahar M, Briegel A, Werner JN, Jensen GJ, Gitai Z. 2010. The metabolic enzyme CTP synthase forms cytoskeletal filaments. *Nat Cell Biol* 12:739–746. <https://doi.org/10.1038/ncb2087>.
  58. Meylan S, Porter CBM, Yang JH, Belenky P, Gutierrez A, Lobritz MA, Park J, Kim SH, Moskowitz SM, Collins JJ. 2017. Carbon sources tune antibiotic susceptibility in *Pseudomonas aeruginosa* via tricarboxylic acid cycle control. *Cell Chem Biol* 24:195–206. <https://doi.org/10.1016/j.chembiol.2016.12.015>.
  59. Rasko DA, Sperandio V. 2010. Anti-virulence strategies to combat bacteria-mediated disease. *Nat Rev Drug Discov* 9:117–128. <https://doi.org/10.1038/nrd3013>.
  60. Miller JH. 1992. A short course in bacterial genetics: a laboratory manual and handbook for *Escherichia coli* and related bacteria. Cold Spring Harbor Laboratory Press, Cold Spring Harbor, NY.
  61. Rahme LG, Stevens EJ, Wolford SF, Shao J, Tompkins RG, Ausubel FM. 1995. Common virulence factors for bacterial pathogenicity in plants and animals. *Science* 268:1899–1902. <https://doi.org/10.1126/science.7604262>.
  62. O’Loughlin CT, Miller LC, Siryaporn A, Drescher K, Semmelhack MF, Bassler BL. 2013. A quorum-sensing inhibitor blocks *Pseudomonas aeruginosa* virulence and biofilm formation. *Proc Natl Acad Sci U S A* 110:17981–17986. <https://doi.org/10.1073/pnas.1316981110>.
  63. Liberati NT, Urbach JM, Miyata S, Lee DG, Drenkard E, Wu G, Villanueva J, Wei T, Ausubel FM. 2006. An ordered, nonredundant library of *Pseudomonas aeruginosa* strain PA14 transposon insertion mutants. *Proc Natl Acad Sci U S A* 103:2833–2838. <https://doi.org/10.1073/pnas.0511100103>.
  64. Dietrich LEP, Price-Whelan A, Petersen A, Whiteley M, Newman DK. 2006. The phenazine pyocyanin is a terminal signalling factor in the quorum sensing network of *Pseudomonas aeruginosa*. *Mol Microbiol* 61:1308–1321. <https://doi.org/10.1111/j.1365-2958.2006.05306.x>.
  65. Ramos I, Dietrich LEP, Price-Whelan A, Newman DK. 2010. Phenazines affect biofilm formation by *Pseudomonas aeruginosa* in similar ways at various scales. *Res Microbiol* 161:187–191. <https://doi.org/10.1016/j.resmic.2010.01.003>.
  66. Loomis WF. 1971. Sensitivity of *Dictyostelium discoideum* to nucleic acid analogues. *Exp Cell Res* 64:484–486. [https://doi.org/10.1016/0014-4827\(71\)90107-8](https://doi.org/10.1016/0014-4827(71)90107-8).
  67. Trinh A, Chen H, Chen Y, Hu Y, Li Z, Siegel E, Linskey M, Wang P, Digman M, Zhou Y-H. 2017. Tracking functional tumor cell subpopulations of malignant glioma by phasor fluorescence lifetime imaging microscopy of NADH. *Cancers* 9:168. <https://doi.org/10.3390/cancers9120168>.